


Evolution of Threshold Displacement Energy in Irradiated Graphite

Filip Vuković,^{1,2,*} Jean-Marc Leyssale,² Philippe Aurel,² and Nigel A. Marks¹

¹*Department of Physics and Astronomy, Curtin University, Perth, Western Australia 6845, Australia*

²*Institut des Sciences Moléculaires, University of Bordeaux, CNRS UMR 5255, 351 Cours de la Libération, 33405 Talence, France*

 (Received 23 July 2018; revised manuscript received 25 October 2018; published 17 December 2018)

Molecular-dynamics simulations are used to compute the threshold displacement energy (E_d) in a series of progressively damaged graphite structures. The E_d values are obtained by a statistically robust probabilistic method using a large number of primary-knock-on-atom events at energies up to 100 eV. No sharp threshold for E_d is observed, and a number of possible definitions are considered. For pristine graphite, the best estimate of E_d is 24 eV. E_d decreases with increasing irradiation damage, dropping by nearly a factor of 2 at a dose of one displacement per atom. For a fully disordered amorphous-carbon structure, E_d is around 5 eV. This evolution of E_d is an important missing ingredient in current estimates of radiation doses in nuclear reactors, which assume E_d is constant over the reactor lifetime, despite substantial structural evolution.

DOI: [10.1103/PhysRevApplied.10.064040](https://doi.org/10.1103/PhysRevApplied.10.064040)

I. INTRODUCTION

It is well known that nuclear graphite undergoes significant structural change over its operational lifetime [1,2]. Neutron moderation results in radiation-damage cascades, thereby creating defects in the graphite lattice. Some of these defects can be removed by annealing [3], such as the infamous Wigner-energy release [4], while others persist. Over time, the accumulating defects significantly alter the microstructure, reducing the degree of crystalline order [5,6] and creating cross-links between layers. These changes affect physical properties such as the thermal conductivity [7] and Young's modulus [8]. Neutron irradiation also leads to dimensional changes on the macroscopic scale [9,10]. Since reactors operate for many decades, there is ongoing scientific and engineering interest to understand the evolution of these structural changes, particularly in relation to extensions of reactor lifetimes.

The standard metric for quantifying radiation damage in reactors and irradiated materials is the number of displacements per atom (dpa) over the irradiation period. The number of dpa is, in turn, dependent on the threshold displacement energy, E_d , which quantifies the minimum kinetic energy to create a permanent defect, such as a Frenkel pair. Despite its importance, E_d is difficult to determine either experimentally or computationally. Experimental measurement of E_d is complicated by multiple uncertainties, including the rapid timescale of defect formation, thermally induced recombination, orientation

effects, and the difficulty of associating a macroscopically observable quantity with an atomic scale rearrangement. Computational studies using molecular dynamics (MD) have faced their own set of difficulties, including the lack of accurate interatomic potentials, small system sizes when density-functional theory is used, and large variability due to insufficient sampling of trajectories. Because of these factors, reported values of E_d for graphite differ by a factor of 7, ranging from 10 to 70 eV. Figure 1 provides a graphical summary of the literature, with experimental results shown in black and simulation studies in red; see Ref. [11] for a discussion of the various methods. Some of this variation can be attributed to orientation effects, with the most extreme value being 780 eV reported by Zobelli *et al.* [12] for displacement along the bond axis. Notably, the value of 60 eV for E_d used by the UK nuclear industry is at the upper end, a value which is “certainly too high,” according to an International Atomic Energy Agency technical document [6]. The same document comments on large reported variations of E_d with crystallographic directions, a situation it describes as “not satisfactory.”

Several years ago a new computational approach was developed for computing E_d using low-energy MD simulation [13]. The method uses robust statistical methods, sampling many different directions, lattices, and atom types to arrive at a probabilistic measure of E_d . Typically some tens of thousands of small MD calculations are required, a computational task that is easily achieved with modern grid and cloud-computing platforms. This statistical approach provides a solid basis with which to study and define the threshold displacement energy, which paradoxically, is not

* filip.vukovic@curtin.edu.au

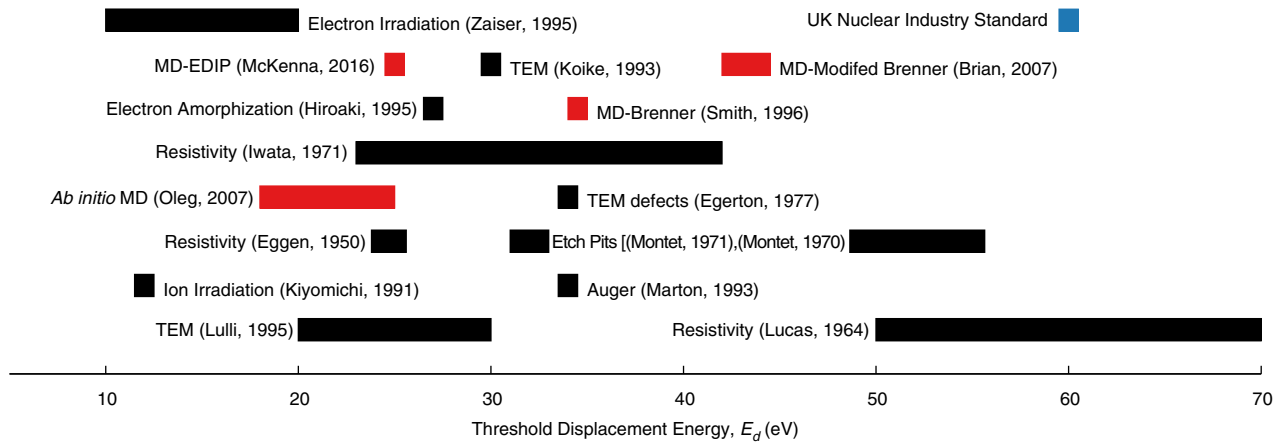


FIG. 1. Literature E_d values for graphite determined by experimental techniques (black bars) and computational methods (red bars). The length of each bar indicates the degree of uncertainty. The blue box indicates the UK-nuclear-industry standard. Reading from left to right and then line by line, the references for all data refer to Refs. [6,11,14–31].

a threshold at all but instead a smoothly varying function of primary-knock-on-atom (PKA) energy.

The problem of determining E_d for nuclear graphite becomes even more complicated given that the structure itself evolves with the dose. To date, simulations have studied only pristine graphite, and previous measurements were performed on either virgin-graphite samples or graphite irradiated at extremely low doses. However, actual graphite cores may experience quite high doses, roughly a few tens of dpa during their lifetimes, and it is unknown how the corresponding structural radiation damage affects E_d . Recently, a computational method combining *in situ* high-resolution-transmission-electron-microscopy (HRTEM) imaging of electron-irradiated graphite with MD simulations was developed to create three-dimensional (3D) structural models of irradiated graphite [32,33]. With use of this image-guided atomic reconstruction (IGAR) method, a series of models with doses up to 1 dpa were produced and validated against various experimental data (HRTEM images, carbon K -edge electron-energy-loss spectra, dose rate, and stored energies), showing good overall agreement [33].

This work combines the statistical approach to E_d with the structural models provided by the IGAR method. With use of the environment-dependent interaction potential (EDIP) for carbon [34,35] and the DIRAC grid-computing infrastructure initially developed for the LHCb experiment at CERN [36,37], a large number of molecular-dynamics simulations of low-energy PKA events are performed for a series of atomistic models at various damage levels ranging from pristine graphite to IGAR structural models at 0.2 and 1 dpa. As a limit for highly damaged graphite, a fully-amorphous-carbon (a -C) model is also considered. To make meaningful comparisons between displacement probabilities (DPs), a generalized

displacement criterion that is suitable for use in damaged and disordered structures is used. Several definitions of the threshold displacement energy are explored, enabling a quantitative discussion of the effect of dose on E_d . This work focuses on the evaluation of displacement probability following a PKA event; other structural changes occurring in a nuclear reactor, such as thermally induced annealing of defects, are not considered. The displacement probabilities sample hundreds of PKA directions and hence accurately capture the average behavior. However, the effect of individual directions (anisotropy) on threshold energy, for which an accurate calculation would require an increase of at least tenfold in the number of simulations, is not considered.

II. METHODOLOGY

The simulations are performed with the EDIP for carbon [34,35], implemented in an in-house molecular-dynamics package. Adapted from an earlier environment-dependent potential for silicon [38], the two- and three-body interactions of the carbon EDIP are mediated by a coordination-based atomic bond order. A key strength of the EDIP is the excellent description of bond making and breaking due to a sophisticated aspherical coordination counting term. In particular, the carbon EDIP accurately predicts the diamond-to-graphite energy barrier, making it ideal for use in disordered carbon systems [39–41] and radiation-damage simulations [11,15].

A. Structural models

The four structural models used in this work are shown in Fig. 2 and constitute a progressive path of increasing structural and textural disorder. Figure 2(a) shows pristine hexagonal (AB) graphite, Figs. 2(b) and 2(c) show IGAR

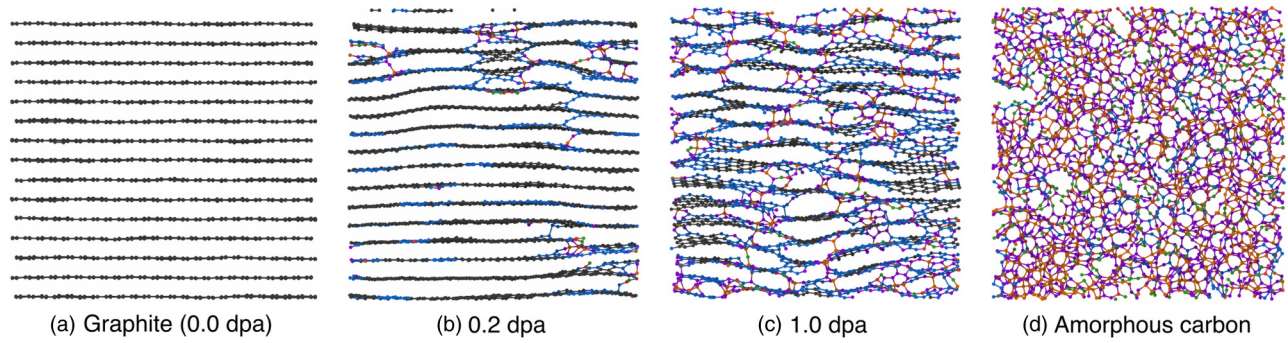


FIG. 2. Cross-section slices (10 Å thick) of the structural models used in the PKA simulations: (a) pristine graphite, (b) IGAR model at 0.2 dpa, (c) time-dependent IGAR model at 1.0 dpa, (d) *a*-C generated by liquid quenching. Atom colors correspond to the local-environment classification outlined in Table I.

models corresponding to different amounts of damage, and Fig. 2(d) shows amorphous carbon. Full details of the four models are described below.

For the pristine-graphite simulations, four lattices are prepared to improve the statistical sampling, with the only difference between lattices being the length of the equilibration time. Each lattice contains 47 520 atoms in a $93.79 \times 88.6 \times 48.58 \text{ \AA}^3$ cell. In Fig. 2(a), only a portion of the simulation cell is shown. To prevent sliding between individual graphene sheets, a plane of atoms perpendicular to the basal plane is held fixed. The fixed atoms are far away from the PKA site (more than 40 Å) and hence do not affect the dynamics.

The two IGAR models in Figs. 2(b) and 2(c) each contain 14 009 atoms and are generated by methods described in Refs. [32,33]. The model in Fig. 2(b) uses of a single HRTEM (002) lattice-fringe image of a nuclear graphite sample irradiated with electrons for 2 min to construct a 3D (HRTEM) potential [32]. This HRTEM potential is then applied together with the adaptive-intermolecular-reactive-bond-order (AIREBO) potential [42]. Starting with a system of randomly arranged atoms in a cubic cell at a density of 2.2 g/cm³ (side length of 50.25 Å), the system is first annealed at high temperature and then slowly cooled to room temperature. On the basis of the 2-min exposure to the electron beam, the estimated dose is 0.2 dpa.

The time-dependent IGAR method [33] is an extension of the original IGAR method. It uses of a sequence of lattice-fringe images, corresponding to progressive electron irradiation of a nuclear graphite sample at room temperature. By constructing a difference HRTEM potential between consecutive images, the method generates a series of structural models as a function of the dose. The structure in Fig. 2(c) corresponds to a total irradiation time of 13 min, for which the estimated dose is 1.0 dpa. Since both of the IGAR models were developed with the AIREBO interatomic potential, it is important to completely relax the coordinates with the EDIP before the

PKA simulations are performed. No significant changes in bonding are observed.

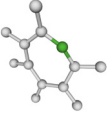
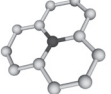
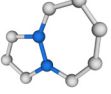
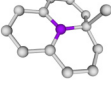
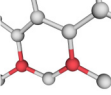
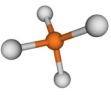
The amorphous-carbon system in Fig. 2(d) is generated by heating of the 1.0-dpa IGAR structure to 8000 K, well above the EDIP melting point. The liquid is equilibrated for many tens of picoseconds, and the mean squared displacement is followed to ensure that the system is highly diffusive. The liquid is rapidly quenched over a period of 0.1 ps to room temperature to create a highly disordered *a*-C network. Before the introduction of the PKA events, an extremely long relaxation is performed to ensure stability of the structure.

B. Atomic environment classification

To quantify progressive irradiation damage in the four structural models, carbon atoms are classified according to their local environment. In bulk-carbon systems, atoms are often described in terms of their coordination, generally assumed to correspond to *sp*, *sp*², and *sp*³ hybridization, corresponding to two, three, and four neighbors, respectively. However, a recent analysis [33] of electron-energy-loss-spectra data for irradiated graphite highlighted the value of splitting the threefold-coordinated atoms into four subcategories. The distinction between categories is made according to the immediate environment (coordination of second neighbors, participation in aromatic rings, etc) and is summarized in Table I. We adopt here the same classification as in Ref. [33], albeit with a slightly different naming scheme [43].

Figure 3 shows the atom-type composition of the four structural models, highlighting the effect of increasing dose and disorder. The fraction of C_3^α atoms (gray symbols; corresponding to a graphite environment) decreases progressively from 100% for graphite to zero for *a*-C. In the irradiated-graphite models, a large fraction of C_3^β atoms (blue symbols) are present. This atom type, corresponding to *sp*² atoms belonging to a nonhexagonal ring, is more common than C_3^α at 1 dpa. Defects induced by radiation

TABLE I. Local-environment classification scheme for carbon atoms. Rings are defined to be composed of only threefold-coordinated atoms.

	Type	Color	Description
	C_2	Green	Twofold- (sp - or sp^2 -radical-) coordinated carbon atom
	C_3^α	Gray	Threefold- (sp^2 -) coordinated carbon atom belonging to three hexagonal rings
	C_3^β	Blue	Threefold- (sp^2 -) coordinated carbon atom bonded to threefold-coordinated neighbors and belonging to at least one nonhexagonal ring (i.e., pentagonal, heptagonal, or octagonal)
	C_3^γ	Violet	Threefold-coordinated carbon atom with at least one fourfold-coordinated neighbor
	C_3^δ	Red	Threefold-coordinated carbon atom with at least one twofold-coordinated or undercoordinated neighbor (and no fourfold-coordinated neighbor)
	C_4	Orange	Fourfold- (sp^3 -) coordinated carbon atom

damage also include interlayer cross-links involving fourfold-coordinated atoms (C_4 ; orange symbols) and unsaturated graphene edges (C_2 atoms; green symbols). These two varieties of defects are also responsible for the numerous C_3^γ and C_3^δ atoms, which are threefold-coordinated atoms bonded to fourfold- or twofold-coordinated atoms, respectively. The population statistics of the a -C structural model can be viewed as a continuation of the trends seen in the other three models (i.e., C_3^α and total threefold-coordinated-atom percentage decreasing with damage and the percentage of other types increasing). The only exception to this trend is the C_3^β population, which has a maximum for the 1-dpa structural model. The total threefold-coordinated-atom percentage of 64% for the a -C model is similar to the percentage from previous EDIP calculations of amorphous carbon [40], where a value of 63% was found at a slightly lower density of 2 g/cm³.

C. PKA simulations

Equilibrium interactions are described with the EDIP, with close-approach interactions described with the

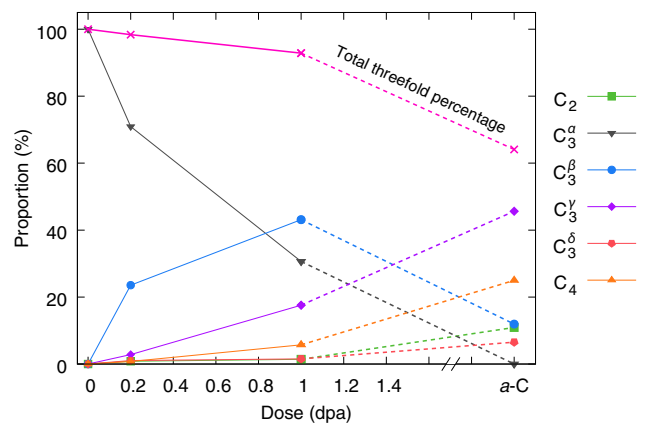


FIG. 3. Population statistics for the four structural models as a function of increasing dose. The broken horizontal axis and the dotted lines indicate no associated dose for amorphous carbon. The magenta data indicate the total percentage of threefold-coordinated atoms, while the other colors denote local atomic environments as defined in Table I.

Ziegler-Biersack-Littmack potential [44]. For intermediate energies, the EDIP pair term is smoothly switched to the Ziegler-Biersack-Littmack potential with use of two Fermi-type switching functions as described in Ref. [15]. Equations of motion are integrated in the microcanonical (NVE) ensemble with a variable-time-step algorithm developed to study high-energy radiation cascades [45]. All structures are equilibrated at room temperature before the PKA events are generated. Simulations are run for 2 ps with PKA energies ranging from 2.5 to 100 eV. After the creation of the PKA event, the net linear momentum is subtracted. Because of the large number of atoms and modest PKA energies, it is not necessary to apply a thermostat; the maximum temperature rise is around 25 K for the highest-energy PKAs. The short timescale of the PKA events is seen in Fig. 4, which shows the maximum kinetic energy as a function of time for 100 simulations of 100-eV PKA events in pristine graphite. Also shown is the average temperature across all 100 simulations. After a fraction of a picosecond, the system reaches equilibrium, demonstrating that 2 ps is more than sufficient to capture the dynamics.

The probabilistic approach to determining E_d involves a large number of MD simulations in which a PKA is given a velocity vector corresponding to a prescribed kinetic energy. For the IGAR and a -C structural models, the PKA is selected at random and prescribed a random direction. Five sets of 100 simulations are performed at each energy, and for each set the probability of a displacement occurring is determined with use of the classification scheme described below. This process yields five values, from which the average and standard deviation are computed. The same block-averaging process is used to compute the PKA range and number of displacements.

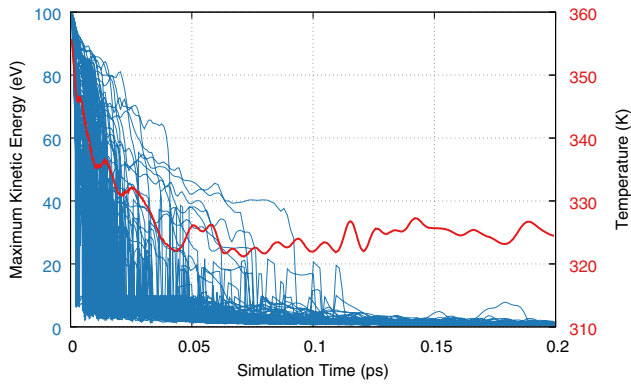


FIG. 4. Time evolution of the kinetic energy and temperature for 100 PKA events in pristine graphite at 100 eV. Thin blue lines (left axis) show the kinetic energy of the most energetic atom at any instant in each simulation, while the thick red line (right axis) shows the instantaneous temperature averaged over all simulations.

For the pristine-graphite structural model, the PKA initial directions are selected from a 100-point solution to the Thomson problem [46,47]. This approach is particularly useful for sampling all directions equivalently in crystalline materials [13,15]. Eight sets of 100 simulations are performed at each energy (four for an α carbon and four for a β carbon) with use of a different equilibrated lattice for each set. As with the disordered structures, the values obtained are used to compute the average and standard deviation. The selected PKAs are in the center of the box (i.e., far from the fixed edges). Note that an α carbon has atoms immediately above and below it in the c direction, while a β carbon does not.

The 1.0-dpa IGAR structure is further studied by our computing the displacement probability according to the local-environment classification. For each atom type and energy, five sets of 100 simulations are performed, and the block-averaging process described above was used. For each simulation a PKA is selected at random from the list of atoms belonging to the type considered. Across all the different calculation types, approximately 120 000 simulations are performed on grid-computing infrastructure using the DIRAC interware framework [36,37].

D. Displacement criterion

An important component of the probabilistic approach is an automated algorithm to determine whether a defect or displacement has occurred. In pristine graphite, the regular crystal structure allows the clear definition of many types of defects, including Frenkel pairs, spiro interstitials, and nonhexagonal rings [9]. For example, a simple vacancy-radius approach was successfully used by Christie *et al.* [15] in their identification of vacancies and interstitials in radiation cascades in graphite. However, considerable difficulties arise in extending the concept of defect formation

to the irradiated-graphite and amorphous-carbon models. In line with the dpa-estimation process in Ref. [33], a relatively strong criterion based on neighbor lists is adopted. For each atom, the number of bonds created (n_c) and the number of bonds broken (n_b) are computed. The atom is then defined as being displaced if $n_c + n_b \geq 2$ and the atom moved further than 0.5 Å from its pre-PKA-event site. With use of this criterion for displacement, it is straightforward to define the DP and number of atomic displacements (N_d) per PKA event of energy E . The former is the probability of a PKA event creating one or more displacements, while the latter is the average number of displacements per PKA.

Visual inspection of many PKA events confirms that this definition provides a sensible definition for all the structural models. This criterion is valid for the creation of point defects in graphite. For instance, the creation of a Frenkel pair results in one atomic displacement, and a Stone-Wales rotation leads to two displacements. As in Ref. [33], the neighbor lists are constructed on the basis of a 1.9-Å cutoff for the interatomic distance, which corresponds to the first minimum of the pair distribution function $g(r)$. The neighbor-based displacement algorithm is compared with a traditional vacancy-radius method in pristine graphite. A test of 100 PKA events across several energies finds that the two methods yield identical identification of displacements.

III. RESULTS

Displacement probabilities of the four structural models are shown in Fig. 5, with the error bars indicating one standard deviation. Similarly to previous studies on oxides [13,48], there is no single threshold above which a displacement is created, but rather there is a gradual increase

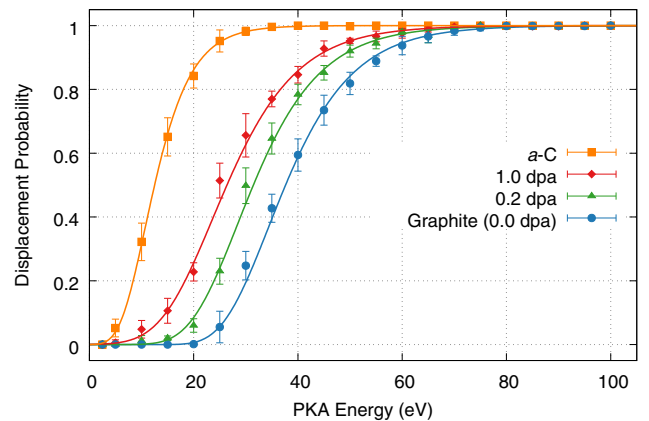


FIG. 5. Displacement probability as a function of PKA energy for a -C (orange), 1.0-dpa irradiated graphite (red), 0.2-dpa irradiated graphite (green), and pristine graphite (blue). Error bars represent one standard deviation. Solid lines denote a generalized logistic fitting function as described in the text.

in the DP. The data also reveal that the DP profile for each structure is unique, with a clear trend of increasing displacement probability with increasing disorder. In the case of pristine graphite, the onset of damage is between 20 and 25 eV, while a 100% probability of displacement does not occur until around 70 eV. The 0.2- and 1.0-dpa structures show a trend similar to that for pristine graphite, albeit with the DP data shifted to lower energies. In contrast, the *a*-C data exhibit a rather different overall shape, with a markedly steeper linear region and a 100% probability of displacement for a PKA energy of approximately 40 eV. This behavior reflects the lack of crystalline order in the amorphous system, which facilitates rearrangement of bonding at comparatively low energies.

Also shown in Fig. 5 is a sigmoidal function that provides a good fit to the data. Many different functional forms are explored, with the best fit being provided by a generalized logistic function that smoothly varies from 0 to 1. This function captures both the tight threshold behavior and the higher-energy curvature of all structures. The fitted displacement-probability curve is of the form

$$DP(E) = (1 - \alpha e^{-\beta E})^{-1/\nu}, \quad (1)$$

with α , β , and ν being free parameters. The fitted values for all four structures are listed in Table II; note that the values of β for the three anisotropic structures are all similar, while for the same structures, the values of α and ν increase with increasing disorder.

While the smooth DP curves present a good overall fit for the displacement data, the soft threshold observed in both the irradiated-graphite system and the *a*-C system makes determination of E_d problematic. A convenient way of defining E_d is to identify the tangent line to the inflection point in the DP curve, with its intercept with the x axis defining E_d . This linear approach is shown in Fig. 6. With this method, pristine graphite yields a value of 25 eV for E_d , while *a*-C has the rather low value of 6 eV. The two irradiated structures yield intermediate values of 19 and 14 eV for 0.2 and 1.0 dpa, respectively. An alternative definition of E_d uses the fitting function itself, in combination with an arbitrary threshold value. Figure 7 presents a graphical summary of these possible definitions of E_d : the linear fit from Fig. 6 and three other values corresponding to threshold DP values of 10%, 50%, and 90%. Regardless of the definition, a general trend of decreasing E_d with

TABLE II. Fitting parameters for the generalized logistic DP curves shown in Fig. 5.

Structure	α	β	ν
Pristine graphite	0.00153	0.11250	0.00003
0.2-dpa graphite	1.65338	0.11562	0.06153
1.0-dpa graphite	2.35758	0.11415	0.15839
Amorphous carbon	0.05951	0.20536	0.00657

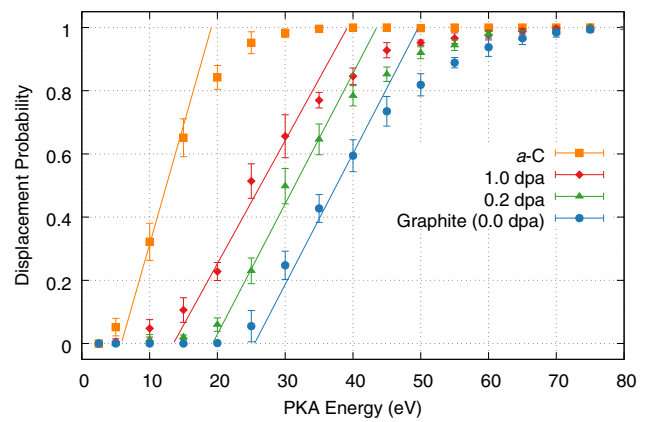


FIG. 6. Linear-analysis procedure used to extract E_d from the data in Fig. 5, where the x intercept defines E_d ; the same color scheme applies.

increasing irradiation damage is apparent. As expected, the lowest value is obtained for the maximally disordered *a*-C structure.

Figure 7 also includes values of E_d computed with the Kinchin-Pease (KP) model [49], which relates the number of displacements to the PKA energy. If we ignore small PKA energies, for which the expression is a piecewise step function, the KP relation can be written in the form $N_d = E/(2E_d)$. As seen in Fig. 8, the number of displacements is indeed a linear function of PKA energy for high energies. To avoid the low-energy region, the linear fit is performed only for data above a DP threshold of 0.9. This procedure yields values of E_d that are slightly lower than for linear-fit and 10% DP approaches, ranging from 22 eV for pristine graphite down to 3 eV for *a*-C. Despite the use of a different displacement criterion, a KP analysis of EDIP

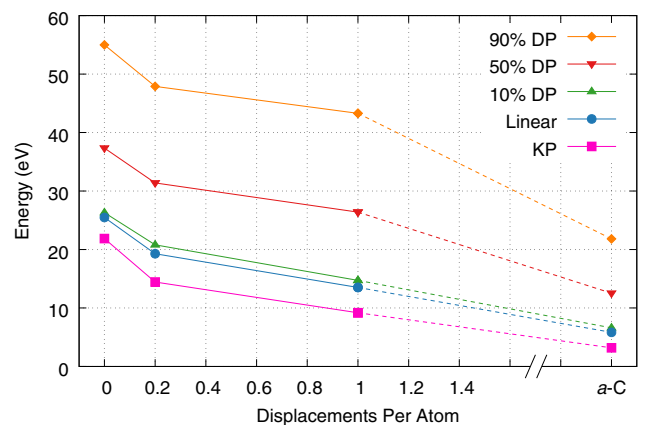


FIG. 7. Values of E_d as a function of damage calculated with five different methods: linear fit (blue; Fig. 6), 10% DP (green), 50% DP (red), 90% DP (orange), and Kinchin and Pease (pink; Fig. 8). The broken axis differentiates *a*-C as a separate structure with no associated irradiation dose.

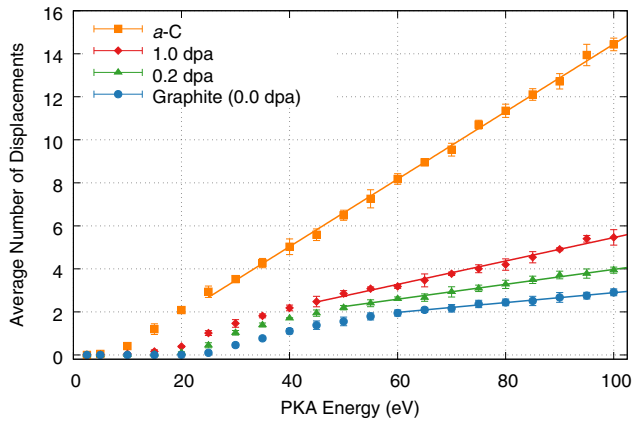


FIG. 8. Average number of displacements as a function of PKA energy for the four structural models; the color scheme in Fig. 5 applies. A linear fit of the KP model is shown as described in the text.

simulations of high-energy cascades in pristine graphite by Christie *et al.* [15] found a similar value of 25 eV.

Another useful piece of information that can be extracted from the data set is the range of the PKA, defined as the distance between the initial and final PKA coordinates. Figure 9 shows the block-averaged PKA range of all the structures, with error bars denoting one standard deviation. All PKA events contribute to the statistics, regardless of whether a displacement occurred or not. As for the DP, there is a low-energy threshold that varies according to the degree of radiation damage. As the PKA energy increases, the range increases in a sublinear manner. From comparison of the different structural models, for a given PKA energy the range increases with the degree of disorder.

Also seen in Fig. 9 is a piecewise power law that provides a good fit to the data, especially at high energies. The functional form is

$$R(E) = \begin{cases} 0, & E \leq \varepsilon, \\ A(E - \varepsilon)^\kappa, & E > \varepsilon, \end{cases} \quad (2)$$

where R is the range, E is the PKA energy, and A , ε , and κ are fitting parameters. The exponent κ ranges between 0.50 and 0.64, similar to values in recent MD simulations by McKenna *et al.* [11], who found the PKA range varied approximately as the square root of PKA energy (see Fig. 4 in Ref. [11]). This type of power-law behavior appears reasonable on physical grounds since the PKA velocity varies as the square root of energy. At the same time, it is important not to overinterpret the trends. For example, the pristine-graphite simulations by Christie *et al.* [15] cover PKA energies between 100 eV and 2.5 keV, and show a linear variation of the PKA range with energy. At the common PKA energy of 100 eV, the range for the different pristine-graphite studies is the same within error bars.

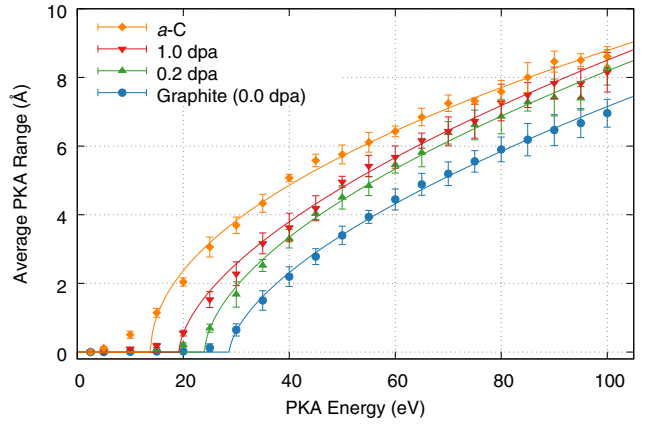


FIG. 9. Average PKA range as a function of PKA energy for the four structural models; the color scheme in Fig. 5 applies. Solid lines are piecewise power-law fits to the data as described in the text.

The finding that all the structural models produce unique DP curves motivated a second set of PKA simulations designed to quantify the effect of the local PKA environment on DP behavior. As described in Sec. II, the 1.0-dpa model is reanalyzed to compute the DP for each atom type. At each PKA energy, 500 simulations are performed for all six atom types in Table I. The results, shown in Fig. 10, with error bars indicating one standard deviation, are fitted with use of the DP function [Eq. (1)] used previously. Each atom type yields a distinct DP curve, with the graphitic C_3^α PKAs being the least likely to form displacements and the C_2 PKAs the most likely. The effect of atom type is substantial and extends across a wide range of PKA energies; for a DP of 50%, the corresponding energy ranges from approximately 15 eV to approximately 30 eV. Even at 90% DP, the energy spread is still nearly a factor of 2.

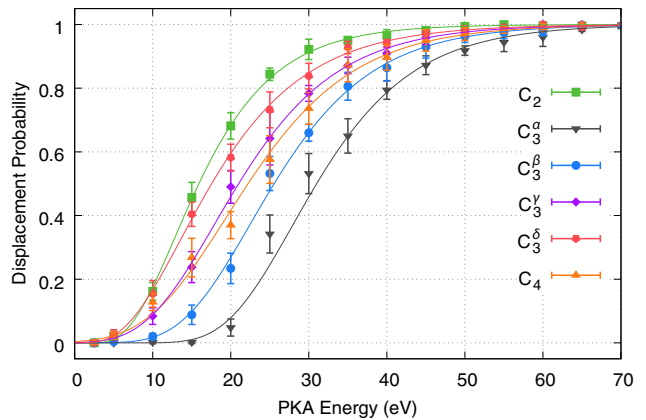


FIG. 10. Data from the PKA study focused on the various atom types are shown as well as fitted displacement-probability curves. The fitted curves and data are colored according to the local-environment classification scheme in Table I.

The large variations between atom types prompted the exploration of a predictive DP approach based on the population statistics for each atom type. In such a scheme, a displacement-probability predictor function, DP^* , is constructed with use of a linear combination of DP curves weighted by atom type. Mathematically, this weighted sum is written

$$DP^*(E) = \sum_i k_i DP_i(E),$$

$$i \in \{C_2, C_3^\alpha, C_3^\beta, C_3^\gamma, C_3^\delta, C_4\}, \quad (3)$$

where k_i is the fractional population for each atom type and DP_i is the corresponding DP function. For the case of the 1.0-dpa structure, the weighted sum reproduces the true DP shown in Fig. 5. This agreement occurs by construction since the two approaches provide different ways of sampling the same statistical quantity. For the 0.2-dpa structure, the weighted-sum approach provides a reasonable representation of the true data. As seen in the inset in Fig. 11, the weighted sum (shown as a solid line) reproduces the shape of the explicit data, albeit with a slight uniform shift to lower PKA energy. While this result is encouraging, the main panel in Fig. 11 shows that the predictive power of the approach is poor for pristine-graphite and α -C structures. For these cases the predicted DP curves do not capture the overall trends, suggesting that the DP is influenced by factors other than local order. For instance, the 0.2-dpa structural model has a texture similar to that of the 1.0-dpa model. In contrast, the isotropic-amorphous-carbon model and crystalline pristine graphite are texturally quite different from both irradiated models.

For completeness, Fig. 12 shows the displacement-probability data and fitted DP curves for the α - and β -carbon PKA in pristine graphite. Given that the local

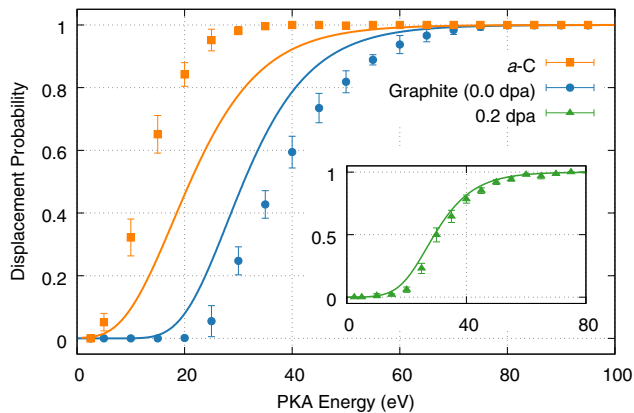


FIG. 11. Predicted DP^* curves for α -C (orange) and pristine graphite (blue) and PKA simulation data from Fig. 5. The inset shows both PKA simulation data and the predicted DP curve for 0.2-dpa irradiated graphite (green).

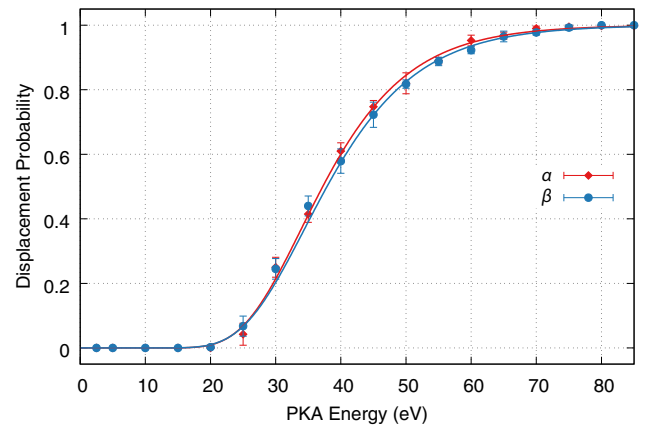


FIG. 12. Displacement-probability data and fitted DP curves for the two symmetry types in pristine graphite: α (red) and β (blue).

symmetries are dissimilar (an α site has atoms above and below it in the c direction, while a β site does not), a variation between the two data sets would not have been surprising. However, Fig. 12 clearly shows that, within error bars, there is no significant difference between α carbon and β carbon.

IV. DISCUSSION AND CONCLUSION

As mentioned in Sec. I, the determination of E_d for pristine graphite has historically proved quite problematic. Figure 1 shows how experimental determinations differ over a wide range, from 10 to 70 eV, while computational values cluster more tightly between 18 and 45 eV. The probabilistic approach used in this work suggests a value in the range 22–26 eV, subject to the caveat that there is no unique measure of E_d . This ambiguity in definition arises because the simulation data demonstrate that there is no sharp displacement threshold from which E_d can directly be determined. Instead, smoothly varying DP curves are obtained, and these need to be interpreted. As seen in Table III, linear extrapolation to zero DP yields a value of 25 eV, while a traditional Kinchin-Pease analysis based on the number of displacements yields a smaller value of 22 eV. An alternative definition based on an arbitrary 10% threshold value for DP yields a slightly higher value of 26 eV. Note that the E_d values from the linear and 10% DP methods are almost the same for all systems, as both analysis methods depend on the fitted DP function.

The values for pristine graphite in Table III are similar to those from *ab initio* MD simulations; Yazyev *et al.* [20] suggested E_d values in the range 18–25 eV, while Susi *et al.* [50] found a value of 21 eV for graphene. The same value of 21 eV was found for large-radius nanotubes with use of density-functional tight binding [51]. This grouping of values builds confidence in the present work and reflects the inherent accuracy of the EDIP interatomic potential,

which has proved itself highly transferable in many different contexts. The similarity also suggests that the 50% and 90% DPs indicated in Fig. 7 are less useful; in the remaining discussion they are explicitly excluded.

Although a substantial E_d literature exists for pristine graphite and related nanocarbons (e.g., graphene and nanotubes; see Ref. [52] for a review), the situation is very different for irradiated graphite and disordered carbons. For these systems there is basically no prior work, and hence the present work provides a significant advance. The major result for irradiated graphite is that E_d reduces substantially with irradiation dose, falling by around a factor of 2 to 10–15 eV at 1.0 dpa, depending on the definition used. Since the procedure for determining dpa values itself depends on the E_d value, a gradual decrease in E_d over a reactor lifetime implies the inferred dpa values become increasingly underestimated as the irradiation damage accumulates. This effect is most clearly seen in Fig. 8, where the number of displacements occurring at a given PKA energy progressively increases with the degree of damage. This means that present dose estimates might need to be modified upward to account for the increased amount of damage relative to the pristine case.

Another benefit of the method developed here is that it provides a framework for quantifying E_d in heavily disordered materials. The *a*-C structural model represents a limiting case of maximal damage in which no resemblance to pristine graphite remains, other than density. For this material, E_d drops to around 5 eV, less than the cohesive energy of the material, indicating that bonding configurations can quite easily be rearranged. Looking more generally, the ability to simulate heavily disordered materials is likely to be valuable in many other materials, particularly in the context of nuclear wastefrom materials. Some wastefrom crystals become amorphous from accumulated radiation damage, while in other situations a glass is deliberately chosen as the starting matrix to avoid problems associated with disorder. In either case, the ability to quantify reliable E_d values is of value. A similar argument applies for mineralogical systems where some crystallites become metamict (i.e., amorphous) over geological time.

As a demonstration of the benefits of the present approach, and in particular, the neighbor-based definition of displacement, the method was applied to a structural

TABLE III. Summary of E_d values (eV) for all structures studied in this work.

Structure	KP	Linear	10% DP
Pristine graphite	22	25	26
0.2-dpa graphite	14	19	21
1.0-dpa graphite	9	14	15
Amorphous carbon	3	6	7
Glassy carbon	7	16	16

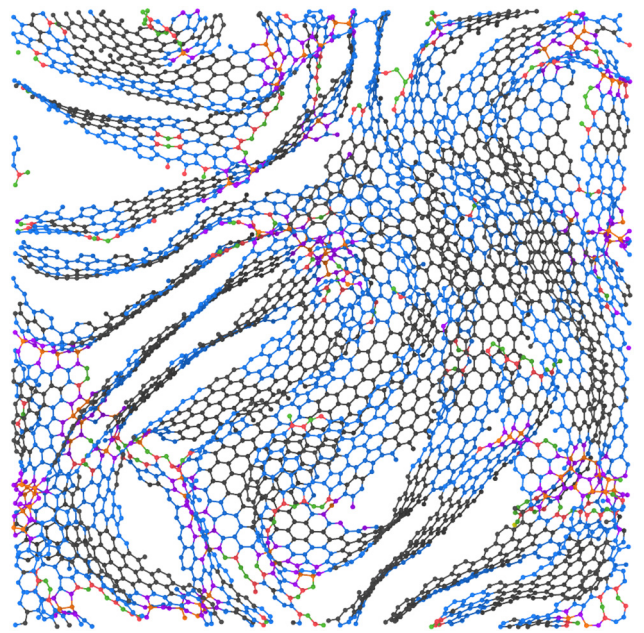


FIG. 13. Cross-section slice (10 Å thick) of the glassy-carbon structural model. Atom colors correspond to the environment classification in Table I.

model for glassy carbon. Also known as “vitreous carbon” or “pyrolytic carbon,” glassy carbon is an important industrial material due to its ability to resist temperatures as high as 3000 °C. The simulations are performed on a 1.5 g/cm³ structural model generated in a study of graphitization by de Tomas *et al.* [41]. The model contains 32 727 atoms in a cubic cell with a side length of 75.8 Å, and is generated by annealing an amorphous-carbon structure for 400 ps at 3000 K. A cross-section slice of the structure is shown in Fig. 13, with atom colors reflecting the local-environment classification. The structure contains 94% threefold-coordinated atoms, and is dominated by C₃^α (45%) and C₃^β (43%) environments, similar in composition to the 1.0-dpa structure.

The glassy-carbon structure is investigated with use of the same statistical analysis and fitting functions, with 500 randomly chosen PKAs and PKA directions at each energy. Figure 14 shows the DP curve, average PKA range, and average number of displacements, all as a function of PKA energy. Also included in Fig. 14 are numerical values of E_d for various definitions; the line in Fig. 14(c) is determined from the inflection point of the fitting function. The three E_d values are similar to the values of 10–15 eV determined earlier for the 1.0-dpa structure, with the caveat that the KP value of 7 eV in Fig. 14 is on the low side. The greatest difference is for the PKA range, where the glassy-carbon values are nearly twice those for the 1.0-dpa structure. Given that the irradiated structures are denser than glassy carbon, 2.2 g/cm³ versus 1.5 g/cm³, this increased PKA range is quite reasonable.

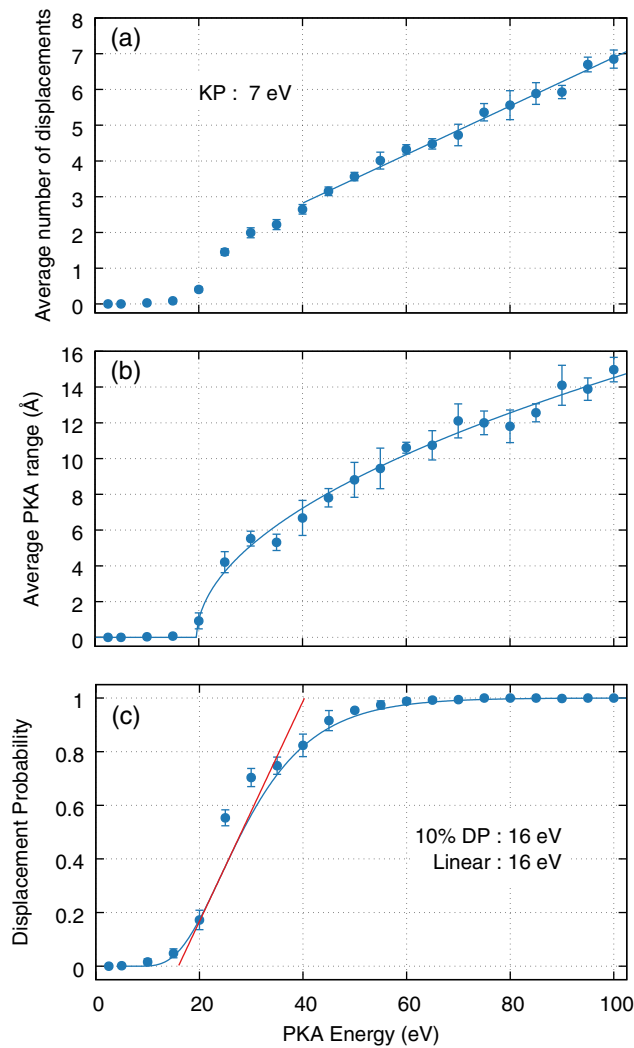


FIG. 14. Results of the simulations for glassy carbon, showing key quantities as a function of PKA energy. (a) Average number of displacements. Also shown is the Kinchin-Pease value of E_d inferred from the fitted slope. (b) Average PKA range, shown with a piecewise power-law fit [Eq. (2)]. (c) Displacement probability, shown with a generalized logistic fit. The red line shows the linear method used to determine E_d .

In summary, the probabilistic approach used in this work provides two key results. Firstly, it generates robust displacement-probability data suitable for determining E_d in pristine graphite, and secondly, it quantifies how E_d varies according to the degree of radiation damage. For pristine graphite, E_d of around 24 eV seems appropriate, considerably less than the UK-nuclear-industry standard of 60 eV. For irradiated graphite, E_d reduces substantially with dose, down to around 12 eV at 1.0 dpa. Since dpa values are themselves dependent on E_d , this result has implications for the definition of the dpa metric in a reactor context. Results are also presented for amorphous carbon and glassy carbon, with E_d values around 6 and 14 eV, respectively. Study of these systems is made possible

due to a robust neighbor-based definition of displacement, making the present method suitable for both crystalline and disordered materials.

ACKNOWLEDGMENTS

This work was conducted as part of the Nicolas Baudin internship program supported by the French embassy in Australia, in conjunction with Campus France. The authors acknowledge the support of France Grilles in providing computing resources on the French National Grid Infrastructure, as well as resources provided by the Pawsey Supercomputing Centre with funding from the Australian Government and the Government of Western Australia.

- [1] R. H. Telling and M. I. Heggie, Radiation defects in graphite, *Philos. Mag.* **87**, 4797 (2007).
- [2] Alain Chartier, Laurent Van Brutzel, Baptiste Pannier, and Philippe Baranek, Atomic scale mechanisms for the amorphisation of irradiated graphite, *Carbon* **91**, 395 (2015).
- [3] P. A. Platonov, E. I. Trofimchuk, O. K. Chugunov, V. I. Karpukhin, Yu. P. Tumanov, and S. I. Alexeev, Annealing of radiation damage in graphite, *Radiat. Eff.* **25**, 105 (1975).
- [4] Lorna Arnold, *Windscale 1957: Anatomy of a Nuclear Accident* (Macmillan Press, London, 1992).
- [5] P. A. Throver and W. N. Reynolds, Microstructural changes in neutron-irradiated graphite, *J. Nucl. Mater.* **8**, 221 (1963).
- [6] B. T. Kelly, Irradiation damage in graphite due to fast neutrons in fission and fusion systems, IAEA-Tecdoc **7**, 176 (2000).
- [7] R. Taylor, R. G. Brown, K. Gilchirst, E. Hall, A. T. Hodds, B. T. Kelly, and F. Morris, The mechanical properties of reactor graphite, *Carbon* **5**, 519 (1967).
- [8] R. Taylor, B. T. Kelly, and K. Gilchirst, The thermal conductivity of fast neutron irradiated graphite, *J. Phys. Chem. Solids* **30**, 2251 (1969).
- [9] M. I. Heggie, I. Suarez-Martinez, C. Davidson, and G. Haf-fenden, Buckle, ruck and tuck: A proposed new model for the response of graphite to neutron irradiation, *J. Nucl. Mater.* **413**, 150 (2011).
- [10] B. J. Marsden, M. Haverty, W. Bodel, G. N. Hall, A. N. Jones, P. M. Mummery, and M. Treifi, Dimensional change, irradiation creep and thermal/mechanical property changes in nuclear graphite, *Int. Mater. Rev.* **61**, 155 (2016).
- [11] A. J. McKenna, T. Trevehan, C. D. Latham, P. J. Young, and M. I. Heggie, Threshold displacement energy and damage function in graphite from molecular dynamics, *Carbon* **99**, 71 (2016).
- [12] A. Zobelli, A. Gloter, C. P. Ewels, G. Seifert, and C. Colliex, Electron knock-on cross section of carbon and boron nitride nanotubes, *Phys. Rev. B Condens. Matter Mater. Phys.* **75**, 1 (2007).
- [13] M. Robinson, N. A. Marks, K. R. Whittle, and G. R. Lumpkin, Systematic calculation of threshold displacement energies: Case study in rutile, *Phys. Rev. B* **85**, 1 (2012).

- [14] Michael Zaiser and Florian Banhart, Radiation-Induced Transformation of Graphite to Diamond, *Phys. Rev. Lett.* **79**, 3680 (1997).
- [15] H. J. Christie, M. Robinson, D. L. Roach, D. K. Ross, I. Suarez-Martinez, and N. A. Marks, Simulating radiation damage cascades in graphite, *Carbon* **81**, 105 (2015).
- [16] J. Koike and D. F. Pedraza, Structural change in graphite during electron irradiation, *Carbon* **279**, 67 (1993).
- [17] Brian D. Hehr, Ayman I. Hawari, and Victor H. Gillette, Molecular dynamics simulations of graphite at high temperatures, *Nucl. Technol.* **160**, 251 (2007).
- [18] Hiroaki Abe, Hiroshi Naramoto, and Chiken Kinoshita, in *Proc. 1994 MRS Fall Meet. Novemb. 28, 1994–Novemb. 30, 1994, Vol. 373* (Boston, Massachusetts, 1995), p. 383.
- [19] R. Smith and K. Beardmore, Molecular dynamics studies of particle impacts with carbon-based materials, *Thin Solid Films* **272**, 255 (1996).
- [20] Oleg V. Yazyev, Ivano Tavernelli, Ursula Rothlisberger, and Lothar Helm, Early stages of radiation damage in graphite and carbon nanostructures: A first-principles molecular dynamics study, *Phys. Rev. B* **75**, 115418 (2007).
- [21] R. F. Egerton, The threshold energy for electron irradiation damage in single-crystal graphite, *Philos. Mag.* **35**, 1425 (1977).
- [22] D. T. Eggen, English Energy Required for Atomic Displacements in Graphite Determined by Electron Bombardment, type Tech. Rep. (United States, 1950).
- [23] G. L. Montet, The threshold curve for the displacement of atoms in graphite, *Carbon* **5**, 19 (1967).
- [24] G. L. Montet and G. E. Myers, Threshold energy for the displacement of surface atoms in graphite, *Carbon* **9**, 179 (1971).
- [25] Kiyomichi Nakai, Chiken Kinoshita, and Atsushi Matsunaga, A study of amorphization and microstructural evolution of graphite under electron or ion irradiation, *Ultramicroscopy* **39**, 361 (1991).
- [26] D. Marton, K. J. Boyd, T. Lytle, and J. W. Rabalais, Near-threshold ion-induced defect production in graphite, *Phys. Rev. B* **48**, 6757 (1993).
- [27] G. Lulli, A. Parisini, and G. Mattei, Influence of electron-beam parameters on the radiation-induced formation of graphitic ions, *Ultramicroscopy* **60**, 187 (1995).
- [28] M. W. Lucas and E. W. J. Mitchell, The threshold curve for the displacement of atoms in graphite: Experiments on the resistivity changes produced in single crystals by fast electron irradiation at 15 K, *Carbon* **1**, 345 (1964).
- [29] G. L. Montet and G. E. Myers, Threshold energy for the displacement of surface atoms in graphite, *Carbon N. Y.* **9**, 179 (1971).
- [30] T. Iwata and T. Nihira, Atomic displacements by electron irradiation in pyrolytic graphite, *Journal of the Physical Society of Japan* **31**, 1761 (1971).
- [31] M. Zaiser and F. Banhart, Radiation-Induced Transformation of Graphite to Diamond, *Phys. Rev. Lett.* **79**, 3680 (1997).
- [32] J. M. Leyssale, J. P. Da Costa, C. Germain, P. Weisbecker, and G. L. Vignoles, Structural features of pyrocarbon atomistic models constructed from transmission electron microscopy images, *Carbon* **50**, 4388 (2012).
- [33] Baptiste Farbos, Helen Freeman, Trevor Hardcastle, Jean Pierre Da Costa, Rik Brydson, Andrew J. Scott, Patrick Weisbecker, Christian Germain, Gérard L. Vignoles, and Jean Marc Leyssale, A time-dependent atomistic reconstruction of severe irradiation damage and associated property changes in nuclear graphite, *Carbon* **120**, 111 (2017).
- [34] N. A. Marks, Generalizing the environment-dependent interaction potential for carbon, *Phys. Rev. B* **63**, 035401 (2000).
- [35] N. A. Marks, Modelling diamond-like carbon with the environment-dependent interaction potential, *J. Phys. Condens. Matter* **14**, 2901 (2002).
- [36] A. Tsaregorodtsev, M. Bargiotti, N. Brook, A. Casajus Ramo, G. Castellani, Ph Charpentier, C. Cioffi, J. Closier, R. Graciani Diaz, G. Kuznetsov, Y. Y. Li, R. Nandakumar, S. Paterson, R. Santinelli, A. C. Smith, M. Seco Miguelez, and S. Gomez Jimenez, DIRAC: A community grid solution, *J. Phys. Conf. Ser.* **119**, 062048 (2008).
- [37] A. Tsaregorodtsev, N. Brook, A. Casajus Ramo, Ph Charpentier, J. Closier, G. Cowan, R. Graciani Diaz, E. Lanciotti, Z. Mathe, R. Nandakumar, S. Paterson, V. Romanovsky, R. Santinelli, M. Sapunov, C. Smith, M. Seco Miguelez, and A. Zhelezov, DIRAC3 - The new generation of the LHCb grid software, *J. Phys. Conf. Ser.* **219**, 062029 (2010).
- [38] Martin Z. Bazant, Efthimios Kaxiras, and J. F. Justo, Environment-dependent interatomic potential for bulk silicon, *Phys. Rev. B* **56**, 8542 (1997).
- [39] N. A. Marks, Thin film deposition of tetrahedral amorphous carbon: A molecular dynamics study, *Diam. Relat. Mater.* **14**, 1223 (2005).
- [40] N. A. Marks, N. C. Cooper, D. R. McKenzie, D. G. McCulloch, P. Bath, and S. P. Russo, Comparison of density-functional, tight-binding, and empirical methods for the simulation of amorphous carbon, *Phys. Rev. B* **65**, 75411 (2002).
- [41] Carla de Tomas, Irene Suarez-Martinez, and Nigel A. Marks, Graphitization of amorphous carbons: A comparative study of interatomic potentials, *Carbon* **109**, 681 (2016).
- [42] S. J. Stuart, A. B. Tutein, and J. A. Harrison, A reactive potential for hydrocarbons with intermolecular interactions, *J. Chem. Phys.* **112**, 6472 (2000).
- [43] The local-area classification was modified for clarity. The subscript now refers solely to the coordination of the atom. The mapping from the old scheme used in previous IGAR work [30] to the new scheme is as follows: $C_1 \rightarrow C_1$, $C_2 \rightarrow C_2$, $C_{3a} \rightarrow C_3^\beta$, $C_{3b} \rightarrow C_3^\gamma$, $C_{3c} \rightarrow C_3^\delta$, $C_4 \rightarrow C_4$, $C_6 \rightarrow C_3^\alpha$.
- [44] J. F. Ziegler, in *Ion Implantation Science and Technology*, edited J. F. Ziegler (Academic Press, Cambridge, Massachusetts, 1988), 2nd ed. p. 3.
- [45] Nigel A. Marks and Marc Robinson, Variable timestep algorithm for molecular dynamics simulation of non-equilibrium processes, *Nucl. Instrum. Methods Phys. Res. B* **352**, 3 (2015).
- [46] J. J. Thomson, On the structure of the atom: An investigation of the stability and periods of oscillation of a number of corpuscles arranged at equal intervals around the circumference of a circle; with application of the results to

- the theory of atomic structure, [London, Edinburgh, Dublin Philos. Mag. J. Sci. **7**, 237 \(1904\)](#).
- [47] David J. Wales and Sidika Ulker, Structure and dynamics of spherical crystals characterized for the Thomson problem, [Phys. Rev. B **74**, 1 \(2006\)](#).
- [48] M. Robinson, N. A. Marks, and G. R. Lumpkin, Structural dependence of threshold displacement energies in rutile, anatase and brookite TiO₂, [Mater. Chem. Phys. **147**, 311 \(2014\)](#).
- [49] G. H. Kinchin and R. S. Pease, Displacement of Atoms in Solid by Radiation, [Rep. Prog. Phys. **18**, 1 \(1955\)](#).
- [50] Toma Susi, Christoph Hofer, Giacomo Argentero, Gregor T. Leuthner, Timothy J. Pennycook, Clemens Mangler, Jannik C. Meyer, and Jani Kotakoski, Isotope analysis in the transmission electron microscope, [Nat. Commun. **7**, 1 \(2016\)](#).
- [51] F. Banhart, J. X. Li, and A. V. Krasheninnikov, Carbon nanotubes under electron irradiation: Stability of the tubes and their action as pipes for atom transport, [Phys. Rev. B **71**, 241408\(R\) \(2005\)](#).
- [52] A. V. Krasheninnikov and K. Nordlund, Ion and electron irradiation-induced effects in nanostructured materials, [J. Appl. Phys. **107**, 071301 \(2010\)](#).